Dynamics of photoexcitation and stimulated optical emission in conjugated polymers: A multiscale quantum-chemistry and Maxwell-Bloch-equations approach

Stefan Schumacher and Ian Galbraith*
Physics Department, School of Engineering and Physical Sciences, SUPA, Heriot-Watt University, Edinburgh EH14 4AS, United Kingdom

Arvydas Ruseckas, Graham A. Turnbull, and Ifor D. W. Samuel
Organic Semiconductor Centre, School of Physics and Astronomy, SUPA, University of St Andrews, North Haugh, St Andrews, Fife KY16 9SS, United Kingdom

(Received 5 November 2009; revised manuscript received 26 March 2010; published 4 June 2010)

We present a general microscopic theory of intense optical pulse propagation in conjugated polymers. The multiscale theory is based on a combination of density-functional theory on the molecular level and many-particle vibronic density matrices which act as a source in Maxwell's equations. The resulting equations are solved nonperturbatively in the light field to study optical amplification and lasing. We illustrate our approach using a polyfluorene material of particular current interest containing a small component of planar (β-phase) chromophores. Significant reshaping of amplified light pulses is found, stemming from the interplay between light propagation and the excitation of numerous vibrational modes. Furthermore a rich dynamic is observed in the amplified spontaneous emission regime with oscillatory structures rooted in the dynamical population and depopulation of lattice modes.

DOI: 10.1103/PhysRevB.81.245407 PACS number(s): 78.47.−p, 42.65.Sf, 78.40.Me, 42.25.Bs

I. INTRODUCTION

Great strides have been made over the last ten years in realizing the potential of cheap, flexible, and easily processed *organic* semiconductors (conjugated polymers).[1–3] The development of early polymer optical amplifiers[4–6] and lasers[7–9] today is following a similar trajectory to that of *inorganic* optoelectronic devices in the 1980s. A key ingredient in advancing polymer photonics and optoelectronics further, is to develop sufficient microscopic theoretical understanding of the relevant nonlinear optical excitation dynamics in these systems. In inorganic semiconductor optoelectronics[10–13] this has been achieved using equation of motion approaches (in different variations of the Semiconductor Bloch Equations[14]). Being based on only a few fundamental material parameters, a largely predictive capability of microscopic theoretical modeling has been achieved for systems ranging from bulk to nanostructures of all dimensionalities.[10–13,15,16] For organic systems, gaining a similarly deep level of understanding and confidence in theoretical modeling would be a significant advance.

Choosing the right theoretical approach to study the optics of a molecular material very much depends on the system at hand but also on the excitation regime and time scales and on the specific questions to be addressed. This work primarily focuses on the regime where (ultrafast) optical amplification is observed. Despite its technological importance, as all-optical amplifiers and lasers constitute basic building blocks of optical communication networks, this regime has not been addressed in previous theoretical work on optics of conjugated polymers.[1,17–23] For the relevant excitation densities, and on the relevant time scales, expanding the optical response into well-defined orders in the external light field[24] can be deemed inappropriate; a theory nonperturbative in the light field[25,26] is needed. Furthermore, the pronounced vibronic substructure of molecular energy levels in organic materials, such as polyfluorenes[1] (in strong contrast to inorganic semiconductor systems), is a fundamental ingredient for organics-based all-optical amplification schemes.[4,5,8] This observation indicates the need for an approach that goes beyond the purely electronic[18,27] dynamics. Further, the appropriate approach should offer extendibility beyond single molecules such that solid-state specific many-particle effects can be addressed.

In the present paper we introduce a multiscale theory for conjugated polymers that is able to meet these requirements. It is based on a density-matrix many-particle theory describing the optically induced vibronic excitation dynamics of the molecular solid-state system under investigation. We combine this approach with density-functional-theory (DFT) calculations for the molecular constituents. The DFT calculations give *ab initio* insight into ground- and excited-vibronic-state properties on the molecular level. This paves the way to formulate a microscopically founded model Hamiltonian including electronic and vibrational degrees of freedom. Starting from this Hamiltonian, the density-matrix equations of motion can be derived and solved together with Maxwell's equations to calculate (nonperturbatively in the external light field) the nonlinear optical excitation dynamics of the system. In this way our approach correctly captures the local microscopic quantum dynamics of the light-matter interaction and simultaneously tracks the wavelength-scale optical pulse propagation.

Motivated by the growing topical interest in conjugated polymer guest-host materials for organic optoelectronics, we demonstrate our general approach on β-phase polyfluorene chromophores (see Fig. 1 for the molecular structure) embedded in a glassy polyfluorene host material.[28–38] In the application of our theory to this system with only dilute chromophores, we neglect the intermolecular Coulomb inter-

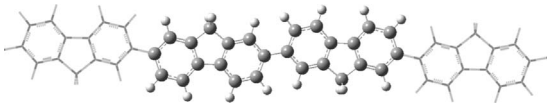

FIG. 1. Molecular structure of a fluorene oligomer in the planar (β-phase) conformation. Explicitly shown is the primitive unit cell consisting of two fluorene units (gray spheres symbolize carbon atoms and light-gray spheres the hydrogen atoms). Periodic continuation of the structure is indicated.

action which simplifies the explicit evaluation of the derived equations of motion. Under conditions where intermolecular Coulomb interaction plays a crucial role, the intrinsic many-particle hierarchy in the density-matrix equations of motion has to be truncated systematically. This can be done, for example, along the lines given in Refs. 39 and 40. For the polyfluorene system investigated here, we present results illustrating the nonlinear optical excitation dynamics in a pump-probe setup and demonstrate conditions where a simple multilevel approach is inadequate to describe these organic systems. We also illustrate how light propagation in a solid-state film leads to radiative coupling of spatially separated chromophores which can drastically influence the system dynamics; for example, giving rise to amplified spontaneous emission (ASE), an important loss mechanism in high-gain extended amplifiers and lasers.[41] Beyond these specific results, our theory provides a general framework for understanding a wide range of phenomena in organic materials, including four-wave mixing, optical amplification, self-induced transparency, photon echo, etc. Also the influence of different organic molecules on these effects can be investigated as the quantum chemistry of the molecular constituents is integral to our approach.

The remainder of this paper is organized as follows. The vibronic density-matrix many-particle theory is developed in Sec. II A, where the master equation including dissipation of vibrational energy, Eq. (8), is the central object of interest for the subsequent calculations. In Sec. II B, we explain how quantum chemical ab initio methods are used to calculate the electronic and vibrational basis states and material parameters entering the solution of Eq. (8). In Sec. III we outline how Eq. (8) can efficiently be solved together with Maxwell's equations and give two illustrational examples of the application of our theory to calculate the nonlinear optical excitation dynamics in a conjugated polymer.

II. THEORY

Quite generally, in modeling the optics of an organic semiconductor material we need to consider an ensemble of conjugated polymer molecules (chromophores) coupled to an external (laser) light field. We assume vanishing overlap of electronic wave functions localized at different chromophores but allow for interchromophore Coulomb interaction and radiative coupling via the propagating light field. We assume that each molecule can be at most singly excited (double excitations are typically not observed in these materials). We restrict this study to the dominant optical transitions close to the fundamental exciton resonance including

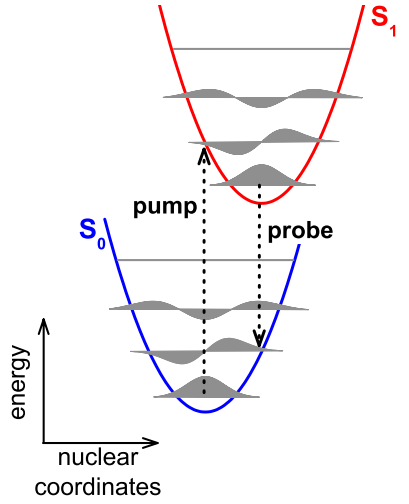

FIG. 2. (Color online) Schematic representation of the ground state, S_0, and first excited singlet state, S_1. Illustrated are the PESs confining the motion of nuclei and the resulting vibrational ladders in each PES. For simplicity the illustration is reduced to only one vibrational degree of freedom and spatial coordinate. The PES displacement between S_0 and S_1 is shown, together with the pump-probe excitation scheme.

the electronic ground (S_0) and first excited singlet (S_1) state of each molecule which can be justified by the large exciton binding energies of typically ≈ 0.5 eV and if the optical excitation frequencies are restricted accordingly. The electronic dynamics on each chromophore is coupled to the vibrational degrees of freedom of the respective molecule. We include this electron-vibrational coupling in Born-Oppenheimer approximation such that it gives rise to $3N-6$ (with N being the number of atoms in the considered molecule) vibrational ladders on top of the electronic states, capturing the inherent vibronic nature of the molecular excitations (schematically depicted in Fig. 2).

A. Polarization and occupation dynamics

We start with the general model Hamiltonian

$$H = H_{\mathrm{mol}} + H_{\mathrm{dipole}} + H_{\mathrm{Coul.}} \tag{1}$$

for an ensemble of molecular chromophores (without permanent electric dipole moments in the ground and excited states). The molecular Hamiltonian in Eq. (1), containing electronic and vibrational degrees of freedom reads

$$H_{\mathrm{mol}} = \sum_{i,\zeta} \left[\varepsilon_{i,\zeta} + \sum_{n} \hbar\omega_{i,n,\zeta} \left(b^{\dagger}_{i,n,\zeta} b_{i,n,\zeta} + \frac{1}{2} \right) \right] c^{\dagger}_{i,\zeta} c_{i,\zeta}. \tag{2}$$

Here, $c^{\dagger}_{i,\zeta}$ ($c_{i,\zeta}$) are creation (annihilation) operators that refer to electronic ground (for $i=0$) and first excited singlet (for $i=1$) state of a molecule at position $\vec{r}_{\zeta}$ with electronic energies $\varepsilon_{0,\zeta}$ and $\varepsilon_{1,\zeta}$, respectively. These operators obey Paulion commutation relations,[42] that is, pairs of operators acting on the same molecule obey Fermion commutation rules, but operators acting on different molecules obey Boson commutation rules. The Hamiltonian (2) of a single molecule is diagonal in the electronic basis states such that no nonradiative

coupling between electronic states is present. The electronic dynamics is coupled to the motion of nuclei in the Born-Oppenheimer approximation. $b^{\dagger}_{i,n,\zeta}$ ($b_{i,n,\zeta}$) are the bosonic creation (annihilation) operators for the n^{th} harmonic oscillator coupled to electronic state i. Through the electronic state dependence of these operators, Eq. (2) also contains the coupling between electronic and vibrational degrees of freedom as detailed in Sec. II B 1. The dipole part of the Hamiltonian

$$H_{\text{dipole}} = \sum_{i\neq j,\zeta} c^{\dagger}_{i,\zeta} c_{j,\zeta} \vec{d}^{\,\zeta}_{ij} \vec{E}(\vec{r}_{\zeta},t) \tag{3}$$

includes the coupling to a time-dependent external light field, $\vec{E}(\vec{r},t)$, in the Franck-Condon approximation. Note, only the electronic degrees of freedom explicitly couple to the light field and the dipole matrix elements $\vec{d}^{\,\zeta}_{ij}$ do not depend on the vibrational state of the molecule. The intermolecular Coulomb interaction[43]

$$\begin{aligned} H_{\text{Coul.}} = &\sum_{\zeta>\zeta'} V^{00}_{\zeta\zeta'} c^{\dagger}_{0,\zeta} c^{\dagger}_{0,\zeta'} c_{0,\zeta'} c_{0,\zeta} + \sum_{\zeta\neq\zeta'} V^{\mathrm{F}}_{\zeta\zeta'} c^{\dagger}_{1,\zeta} c^{\dagger}_{0,\zeta'} c_{1,\zeta'} c_{0,\zeta} \\ &+ \sum_{\zeta\neq\zeta'} V^{\mathrm{X}}_{\zeta\zeta'} c^{\dagger}_{1,\zeta} c^{\dagger}_{0,\zeta'} c_{0,\zeta'} c_{1,\zeta} + \sum_{\zeta>\zeta'} V^{\mathrm{XX}}_{\zeta\zeta'} c^{\dagger}_{1,\zeta} c^{\dagger}_{1,\zeta'} c_{1,\zeta'} c_{1,\zeta} \end{aligned} \tag{4}$$

is also included in the Franck-Condon approximation and contains, in order of their appearance in Eq. (4), a ground-state shift, Förster-type interaction of excitations, exciton and biexciton shifts, mediated by the respective intermolecular Coulomb matrix elements $V^{00}_{\zeta\zeta'}$, $V^{\mathrm{F}}_{\zeta\zeta'}$, $V^{\mathrm{X}}_{\zeta\zeta'}$, and $V^{\mathrm{XX}}_{\zeta\zeta'}$.

In the following, we investigate the nonlinear optical excitation dynamics of a system described by the Hamiltonian (1). Generally, doing optics theoretically, involves solving Maxwell's equations

$$\vec{\nabla}\times\vec{E} = -\frac{\partial}{\partial t}\vec{B}, \tag{5}$$

$$\vec{\nabla}\times\vec{B} = \mu_0\epsilon_0\epsilon_b\frac{\partial}{\partial t}\vec{E} + \frac{\partial}{\partial t}\vec{P}, \tag{6}$$

where we have assumed a system without presence of free charges or currents, respectively. ε_b is the static background dielectric function. Solving this set of coupled equations of motion in space and time requires knowledge of the source term, the optically induced macroscopic polarization $\vec{P} = \vec{P}(\vec{r},t)$. In the following, we calculate $\vec{P}$ from the Hamiltonian (1) and simultaneously solve Eqs. (5) and (6). In the present work, we apply the general theory described thus far to the concrete example of light fields propagating through dilute molecular chromophores (in our case realized by β-phase fluorene chromophores embedded in a host system of α-phase fluorene, see Sec. II B for details). We assume that in such a system, no intermolecular Coulomb interaction needs to be considered, thus intermolecular coupling is exclusively by the propagating light field. More general scenarios, where the intermolecular Coulomb interaction needs included, can also be studied based on the present theory.[39,40] Here, the macroscopic polarization $\vec{P}$ can be calculated as the expectation value of the dipole operator as a sum over independent (apart from coupling via the light-field) contributions from all the molecules ζ present in the system

$$\vec{P}(\vec{r},t) = \sum_{\zeta}\sum_{i\neq j,\nu,n} \vec{d}^{\,\zeta}_{ij} \langle c^{\dagger}_{i,\zeta} c_{j,\zeta} b^{\dagger\nu}_{0,n,\zeta} b^{\nu}_{0,n,\zeta}\rangle_{\zeta} \delta(\vec{r}-\vec{r}_{\zeta}), \tag{7}$$

where again the Franck-Condon approximation was used. Evaluating Eq. (7) involves a summation over the elements of the vibronic density matrix $\langle c^{\dagger}_{i,\zeta} c_{j,\zeta} b^{\dagger\nu}_{0,n,\zeta} b^{\nu}_{0,n,\zeta}\rangle_{\zeta}$ describing the optically excited system dynamics at each molecular site $\vec{r}_{\zeta}$. The dynamics of the density operator ρ_{ζ} describing a molecule at position $\vec{r}_{\zeta}$ is determined by the Hamiltonian H_{ζ} describing the respective molecule and is governed by the master equation

$$\hbar\dot{\rho}_{\zeta} = -i[H_{\zeta},\rho_{\zeta}] + \dot{\rho}_{\zeta,\text{diss.}}. \tag{8}$$

In Sec. III we solve this master equation in matrix representation numerically in the time domain together with Maxwell's equations, Eqs. (5) and (6). We note that the direct solution of these coupled partial differential equations captures the nonlinear spatiotemporal photoexcitation dynamics of the studied conjugated polymer system including nonperturbative coupling of electronic degrees of freedom to both the light field and the vibrational oscillators.

Dissipation of vibrational energy to the surrounding solid-state environment is included in the Markovian approximation via coupling of each molecule independently to a large heat sink. On an operator level this dissipative part $\dot{\rho}_{\text{diss.}}$ for each harmonic oscillator mode included is of the Lindblad form[44,45] (indices distinguishing different molecules, oscillators, and electronic states, respectively, are suppressed for clarity)

$$\dot{\rho}_{\text{diss.}} = -\sum_{nm} h_{nm}(\rho L_m L_n + L_m L_n \rho - 2L_n \rho L_m) + \text{H.c.}. \tag{9}$$

For each harmonic oscillator, this general expression can be specified with

$$L_0 = b, \quad L_1 = b^{\dagger}, \quad h_{01} = -\frac{\gamma}{2}(\bar{n}+1), \quad h_{10} = -\frac{\gamma}{2}\bar{n}$$

and $h_{nm}=0$ for all other n and m, which leads to

$$\begin{aligned} \dot{\rho}_{\zeta,\text{diss.}} = \frac{\gamma}{2}\Big\{ &\sum_{i,n}(2\bar{n}_{\zeta,i}+1)[b^{\dagger}_{i,n,\zeta} b_{i,n,\zeta}\tilde{\rho}_{\zeta} + \tilde{\rho}_{\zeta} b^{\dagger}_{i,n,\zeta} b_{i,n,\zeta}] \\ &+ 2\bar{n}_{\zeta,i}[\tilde{\rho}_{\zeta} - b_{i,n,\zeta}\tilde{\rho}_{\zeta} b^{\dagger}_{i,n,\zeta} - b^{\dagger}_{i,n,\zeta}\tilde{\rho}_{\zeta} b_{i,n,\zeta}] \\ &- 2b_{i,n,\zeta}\tilde{\rho}_{\zeta} b^{\dagger}_{i,n,\zeta}\Big\} \end{aligned}$$

with $\tilde{\rho}_{\zeta}=\rho_{\zeta}+\rho^{\dagger}_{\zeta}$. Here, $\bar{n}_{\zeta,i}$ is the mean number of excitations in the reservoir damping the oscillator and γ is the associated decay constant. From this, vibrational relaxation within each potential-energy surface (PES) follows; nonradiative transitions between different PESs are neglected. In addition to the dephasing induced by this relaxation, we include a pure dephasing such that a realistic homogeneous linewidth of vibronic transitions is achieved in comparison with experimental data (see also Sec. II B). Detailed expressions for relaxation and dephasing terms are given in the Appendix.

TABLE I. Summary of parameters used in the calculations. Note that the value used for γ can be different from the value given here as noted in the results section.

Parameter	Value
$\varepsilon_1-\varepsilon_0$	2.776 eV
Transition dipole $\lvert\vec{d}\rvert$	4.8875 eÅ
Oscillator energies: $\hbar\omega_1$, $\hbar\omega_2$, $\hbar\omega_3$	138, 190, 378 meV
Oscillator displacements: β_1, β_2, β_3	$\sqrt{0.45}$, $\sqrt{0.42}$, $\sqrt{0.11}$
Chromophore density[a]	0.43×10^{19} cm^{-3}
Refractive index[b] $n_{\mathrm{bg}}=\sqrt{\varepsilon_b}$	1.59
γ_{pure}	$\hbar/(44$ fs)
γ	$\hbar/(1$ ps)

[a]Reference 48.
[b]Reference 49.

The bath temperature and with it the mean occupation $\bar{n}_{\zeta,i}$ in each oscillator mode can be varied to study the temperature dependence of optical spectra and nonlinear excitation dynamics.[38]

We note that the inclusion of dissipative phenomena can be extended beyond the treatment in the present work (cf., e.g., Ref. 46). Additional contributions can be included in the master equation, Eq. (8) on different levels of the theory, if needed, also beyond a Markovian treatment, e.g., to allow for nonradiative recombination of electronic excitations. Furthermore, if known to play an important role in the dynamics, additional electronic states (e.g., higher-lying states) can be included in the theory.[47] In its present form the theory is restricted to systems where the dynamics of electronic and vibrational degrees of freedom can approximately be decoupled (Born-Oppenheimer approximation) and where the Franck-Condon approximation is applicable to optically induced and Coulomb-induced transitions between electronic states. The theory is not applicable to systems where these approximations are strongly violated and extensions that go beyond Born-Oppenheimer or Franck-Condon approximation will be computationally difficult to incorporate.

To conclude this section, we note that our approach is generally in analogy to the derivation of the well-known Semiconductor Bloch Equations[14] for inorganic semiconductor systems. However, in contrast to extended Bloch-type basis states we chose states that are localized at the molecular sites as the quantum-mechanical basis to work in. Also, we explicitly include the vibrational modes at each molecular site to account for the strongly vibronic (electronic and vibrational) nature of optical excitations in organic semiconductor materials. In Sec. III we will give explicit examples how the electron-vibrational coupling distinguishes the nonlinear excitation dynamics from purely electronic excitations.

In the following, we apply the formalism developed in this section to a specific conjugated polymer system, a polyfluorene system. Before we proceed to study its nonlinear photoexcitation dynamics in Sec. III, in the following section we discuss how the required material parameters are obtained from quantum-chemical calculations (parameters are summarized in Table I).

B. Vibronic states and spectra

In recent years, there has been a great interest in polyfluorene systems containing a small content of planar, so-called β-phase, fluorene molecules (the molecular structure is illustrated in Fig. 1). Although the planar molecular conformation is not stable for an isolated gas-phase molecule, it has been observed for a number of oligo- and polyfluorene systems where it is stabilized in a solid-state environment.[28–35] Due to its distinct (from the usual glassy phase of polyfluorenes) spectroscopic properties, the β phase has among other things been discussed as a promising candidate for electrically pumped organic laser systems.[35] Currently, the content of β phase in polyfluorene systems can, up to a certain degree, even be experimentally controlled.[29,50] For this system, we have done a detailed quantum-chemical analysis of the S_0 and S_1 electronic states and the respective vibrational frequencies and oscillator modes. This analysis gives the input parameters ($\varepsilon_{i,\zeta}$, $\omega_{i,n,\zeta}$, $\vec{d}^{\zeta}_{ij}$, and $\beta_{i,n,\zeta}$) required to evaluate the density-matrix theory formulated in the previous section.

We have performed ab initio quantum-chemistry calculations for a single fluorene octamer using GAUSSIAN03. We calculate equilibrium geometries of S_0 and S_1, vibrational normal modes and frequencies, and vertical transition energies and transition dipole moments. Transition energies and dipoles are calculated with time-dependent DFT (TD-DFT) for the optimized S_0 (optimized on the DFT level) and S_1 (optimized on the configuration interaction with single excitations (CIS) level) geometries, respectively. For the calculation of vibrational modes and frequencies, we have optimized the S_0 and S_1 geometries on Hartree-Fock (HF) and CIS level of theory,[21] respectively, using tight optimization criteria, and then done a subsequent HF vibrational analysis in the S_0 geometry. Following Ref. 51, the vibrational frequencies obtained from the HF calculations were scaled with a factor of 0.9. The B3LYP functional was used with the 6-31G basis set for all TD-DFT calculations and the 3-21G basis set for geometry optimizations and vibrational analyses. The computational accuracy achieved with the above choice of level of theory, has been shown to yield ground- and excited-state properties such as molecular geometries and transition energies of oligofluorenes that are in good agreement with available experimental data.[36,52] However, we note that in other conjugated polymer systems, especially where long-range charge-transfer effects play an important role in the electronic excitations, e.g., in certain copolymer systems,[53,54] DFT-based methods may have to be used with care. For such systems, more advanced functionals where also long-range contributions to the electronic exchange interaction are included, such as CAM-B3LYP, are expected to give more reliable results. Electronic parameters following from our calculations are the transition dipole $\lvert\vec{d}\rvert=4.8875$ eÅ, which is the average of absorption and emission dipole obtained from the quantum-chemistry calculation so that it can be used as input in the Hamiltonian (1), and $\varepsilon^{\Delta}_{\mathrm{el}}=\varepsilon_1-\varepsilon_0=2.776$ eV, which is obtained from the calculated vertical transition energies as $\varepsilon^{\Delta}_{\mathrm{el}}=(\epsilon^{\mathrm{vert}}_{S_0}+\epsilon^{\mathrm{vert}}_{S_1})/2$. The extraction of vibrational parameters is discussed in detail in the following section and the parameters are summarized in Table I.

1. Linear vibronic optical spectra

We evaluate the equations of motion in Eq. (8) in the basis of the vibrational oscillators of the electronic ground state, S_0. We assume that the PES of the excited electronic state (S_1) is displaced relative to the ground state (S_0) PES along the normal mode coordinates of the ground state (cf. sketch in Fig. 2). Negligible distortion of oscillators upon photoexcitation is assumed ($\omega_{0,n,\zeta}=\omega_{1,n,\zeta}$) and a Duschinsky matrix close to unity (for generalization see, e.g., Ref. 55). Then, on the operator level, the excited-state operators follow from the ground-state operators by adding a dimensionless displacement $\beta_{i,n,\zeta}$ for each oscillator mode n (Ref. 56)

$$b_{i,n,\zeta}^{(\dagger)} \rightarrow b_{0,n,\zeta}^{(\dagger)} + \beta_{i,n,\zeta}. \tag{10}$$

We determine these displacements $\beta_{i,n,\zeta}$ from ab initio quantum-chemistry calculations as outlined below.

We note that explicit insertion of Eq. (10) into the Hamiltonian (1) introduces a coupling of electronic and vibrational degrees of freedom linear in $\beta_{i,n,\zeta}$, appropriate for the conjugated polymer systems investigated.[17] A distortion of the oscillators upon photoexcitation would lead to contributions nonlinear in this coupling. In matrix representation, in the basis of the S_0 oscillator states, the electron-vibrational coupling generates off-diagonal elements in the molecular part of Eq. (1). A basis change that diagonalizes this part of the Hamiltonian, i.e., the transition to vibronic basis states, brings the Franck-Condon factors explicitly into the dipole-coupling part of Eq. (1). This transition makes the interpretation of linear optical spectra most intuitive.

The vector containing the oscillator displacements in each normal mode

$$\vec{\beta} = A^{-1}\vec{G}_{\Delta}\sqrt{\frac{M\omega}{2\hbar}} \tag{11}$$

can be obtained from the difference in ground- and excited-state equilibrium geometries $\vec{G}_{\Delta}$ projected onto the complete set of normal mode coordinates (stored in the columns of A).[21] Using Eq. (10), the displacements $\vec{\beta}$ can directly be used as input parameters in the Hamiltonian (1). For the following analysis it is also useful to define the Huang-Rys (HR) factor, R_n, for each oscillator mode n, $R_n=(\beta_n)^2$, and the Franck-Condon factors[57]

$$F_{\nu,\nu'}(n) = \exp\left(-\frac{\beta_n^2}{2}\right)\sqrt{\frac{\nu!}{\nu'!}}\beta_n^{\nu'-\nu}L_{\nu}^{\nu'-\nu}(\beta_n^2) \tag{12}$$

giving the overlap of the vibrational state ν of S_0 with the vibrational state ν' of S_1. The Laguerre polynomial $L_{\nu}^{\nu'-\nu}(\beta_n^2)$ is given by

$$L_{\nu}^{\nu'-\nu}(\beta_n^2) = \sum_{i=\max(0,\nu-\nu')}^{\nu} \frac{(-1)^i\nu'!(\beta_n^2)^i}{i!(\nu-i)!(\nu'-\nu+i)!}. \tag{13}$$

Based on the approximations summarized above, we can calculate linear absorption spectra using the full vibrational data obtained from the quantum-chemistry calculations. At zero temperature, the frequency-dependent linear absorption of a single molecule is

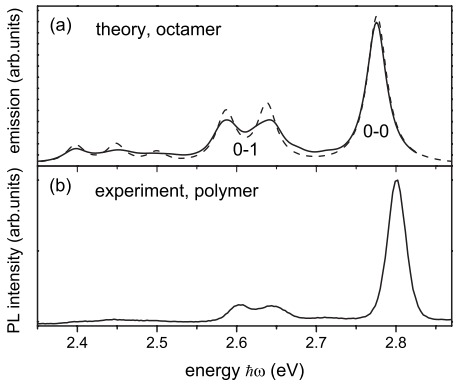

FIG. 3. (a) Calculated low-temperature linear vibronic emission, $-\alpha(\omega)\cdot\omega^2$, of a vibrationally relaxed planar (β-phase) fluorene octamer in full occupation inversion [solid line with $\alpha(\omega)$ defined in Eq. (14)]. Dashed line: same as solid line but based on a simplified calculation including three effective vibrational modes as defined in Sec. II B 2. (b) Experimental photoluminescence spectrum of β-phase polyfluorene at 77 K (for experimental details see Ref. 36).

$$\alpha(\omega) \sim \omega\cdot\mathrm{Im}\{\chi(\omega)\} = \omega\cdot\mathrm{Im}\{P(\omega)/E(\omega)\}$$
$$\sim \mathrm{Im}\left\{\sum_{\{\nu_n^0\},\{\nu_n^1\}} \frac{\omega\cdot|\vec{d}|^2(f_{\{\nu_n^0\}}^{S_0}-f_{\{\nu_n^1\}}^{S_1})\prod_n|F_{\nu_n^0,\nu_n^1}(n)|^2}{\hbar\omega-\varepsilon_{\mathrm{el}}^{\Delta}-\sum_n[\hbar\omega_n(\nu_n^1-\nu_n^0)]+i\gamma_{\mathrm{pure}}}\right\} \tag{14}$$

with $\{\nu_n^i\}=\nu_1^i,\ \nu_2^i,\ldots,\nu_N^i$ and $\nu_j^{i=0,1}=\{0,1,\ldots\}$. The $f_{\{\nu_n^i\}}^{S_i}$ denote the static (in the linear optical regime) occupations of each vibronic level and γ_{pure} is the width of each of the homogeneous Lorentzian lines in the vibronic spectrum (for simplicity, here γ_{pure} is the same for all the oscillator modes n). Note that apart from the finite linewidths, Eq. (14) formally follows from linearization of Eq. (7) in the external field E and subsequent Fourier transformation to the frequency domain. We have evaluated Eq. (14) for the case of complete occupation inversion such that the occupation of the vibrational ground state of S_1 is unity ($f_{\{\nu_n^1\}}^{S_1}=1$ if $\nu_n^1=0\,\forall\,n$; all other occupations zero). In this case the absorption $\alpha(\omega)$ is negative (and thus corresponds to gain) and can be related to the spontaneous emission if the frequency dependence of spontaneous fluctuations in the vacuum field is taken into account. In Fig. 3 we compare $-\alpha(\omega)\cdot\omega^2$ with the photoluminescence of β-phase polyfluorene at low temperatures. Despite the finite length of the oligomer, exceptionally good agreement of absolute energies and spectral features is found between theory and experiment (also compare Refs. 29, 30, and 58). The homogeneous linewidth in the calculations was $\gamma_{\mathrm{pure}}=\hbar/44$ fs (we use this value for the pure dephasing throughout this work).

2. Effective vibrational modes

In the calculation of linear optical spectra according to Eq. (14) sufficiently many vibrational modes have been taken into account to reach convergence for the results shown in Fig. 3. However, about 50 modes that couple most

strongly to the electronic system (identified by the largest oscillator displacement) need to be included for the fluorene octamer under investigation. This is about 10% of the total number of vibrational modes in this molecule. Thus, despite the apparently simple appearance of the spectra in Fig. 3, starting from the true ab initio quantum-chemistry data, too many vibrational modes would have to be considered to directly calculate the nonlinear system dynamics from Eq. (8). Note that the dimension of the matrix representing the Hamiltonian H_ζ in Eq. (8) is $\sim 10^N$, if N is the number of oscillator modes included and assuming that ten oscillator basis states per mode are needed to achieve a numerically accurate description. To reduce the number of modes needed in the dynamics calculations, we choose to define a small number of effective vibrational modes. An algorithm to define these modes based on the full information of the vibrational analysis can be defined as follows. The qualitative structure of the linear optical spectra determines the number of effective modes needed and their frequencies. Then, the HR factors of the effective modes are calculated from the HR factors of the real modes as[59] $R_{\text{eff}}=\Sigma_n R_n$ in frequency intervals around the frequencies of the chosen effective modes. Figure 3 shows an example where three effective modes at energies 138, 190, and 378 meV with oscillator displacements $\sqrt{0.45}$, $\sqrt{0.42}$, and $\sqrt{0.11}$, respectively, have been included. The appearance of the two lower-frequency modes is typical for conjugated polymer systems and can be traced back to stretching motions of single and double carbon-carbon bonds. The mode with frequency 378 meV involves oscillation of the light hydrogen atoms and takes some additional oscillator strength away from the 0-0 line and slightly improves the overall agreement with the full spectrum. However, we note that this mode only makes a very minor contribution to the calculations of the system's nonlinear excitation dynamics (see Sec. III) and that this mode may not be active when the molecules are embedded in a solid-state environment. We find no low-frequency vibrations with strong coupling to the electronic degrees of freedom in the β-phase molecule considered here. Consequently, the (homogeneous) line widths of the 0-0 vibronic peaks of the full and effective-mode calculations almost perfectly agree. All other effective resonances come out slightly narrow compared to the full result. Nevertheless, this analysis indicates that for the linear optical properties of the system, introduction of only few effective modes derived from the quantum-chemistry calculations with a small number of free parameters can be justified. Given the small number (three) of effective modes, the overall resemblance of the full spectrum achieved is quite remarkable (note that the same pure dephasing was used as for the full calculation). Since the dominant contributions in the electron-vibrational coupling found here are related to stretching motions of single and double carbon-carbon bonds, we expect the effective-mode approach to have validity in a wide range of conjugated polymers.[59] However, where strong coupling to a low-frequency vibrational mode exists or where anharmonicities play an important role, the respective vibrational modes will have to be treated with care.[60] In the remainder of this paper, we use these effective vibrational modes as input for the nonlinear excitation dynamics calculations. Possible differences between the full and the effective-mode nonlinear dynamics of the system should be analyzed in more detail in future work. As detailed in the Appendix, the relaxation of vibrational quanta included in the system dynamics gives rise to additional—albeit much smaller—contributions to the homogeneous linewidths.

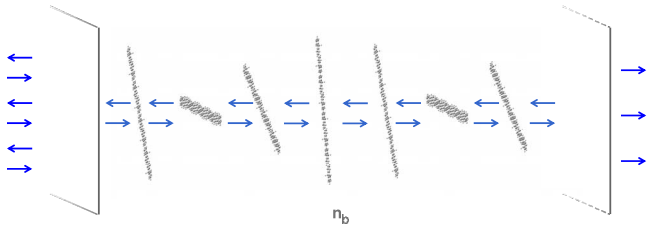

FIG. 4. (Color online) Illustration of the spin-coated organic semiconductor film. In the calculations, the chromophore layers are uniformly spaced and the orientation of the linearly polarized transition dipoles is uniformly distributed about the direction of propagation.

III. NONLINEAR PHOTOEXCITATION DYNAMICS—RESULTS AND DISCUSSION

In this section we discuss examples illustrating the nonlinear excitation dynamics of a molecular system following from the explicit time-domain solution of Eqs. (5), (6), and (8). In the numerical evaluations, the density-matrix equations of motion are solved within the rotating wave approximation using a fourth-order Runge-Kutta algorithm which provides accuracy and stability of the solutions up to long (nanosecond) time scales.[13] The oscillator basis states are truncated for high occupation numbers (typically ≈ 10) such that numerical convergence of the results is achieved. All calculations are for zero temperature, $T=0$.

We study dilute β-phase oligo- or polyfluorene chromophores embedded in a glassy polyfluorene host system. Spatially separated chromophores are coupled via the propagating light field. As an important solid-state specific effect following from this radiative coupling, amplified spontaneous emission will be discussed in Sec. III B. We study solid-state films that have been spin coated so that the molecular dipoles are all oriented within the plane of the film (cf. Fig. 4). For clarity, we neglect inhomogeneous broadening such that all the chromophores considered are identical (apart from their position and orientation in space). However, we note that inclusion of an imhomogeneous broadening, e.g., caused by a Gaussian distribution of electronic excitation energies, is straightforward as the dynamics at each chromophore site is explicitly calculated. We consider an incoming optical field in normal incidence with circular light polarization. If the film is infinitely extended in the plane, and if spontaneous emission effects are not relevant in directions other than the propagation direction of the incoming field, the propagation of the optical field behaves effectively one dimensionally, $\vec{E}(\vec{r},t)=\vec{E}(t)e^{-kz}$; the light "sees" a similar physical situation everywhere in the transverse plane.

Keeping these physically realistic simplifications in mind, light propagation can explicitly be considered and efficiently

solved within a one-dimensional time-dependent transfer-matrix formalism.[15,61,62] In the transfer-matrix formalism, at each chromophore layer i, part of the incoming field on each side is reflected. The reflected field is determined by the optically induced polarization of chromophore layer i which is assumed to be infinitely thin in propagation direction. This leads to so-called local-field corrections,[63] modifying the effective optical field interacting with each chromophore/molecule. The strength of interaction of the light field with the film is effectively determined by the number of chromophores in propagation direction, their dipole-matrix elements, and the in-plane density of chromophores. For more details on the explicit application of a time-dependent transfer-matrix formalism to a multilayer system, see, e.g., Ref. 61. In the numerical simulations the chromophores are uniformly spaced in propagation direction and the orientations of the linear chromophore dipoles are equally distributed about the propagation direction (cf. Fig. 4). To concentrate on the propagation effects that are inherent and not caused by multiple reflections between the surfaces of the material, we have switched off air-to-material transitions in the background refractive index, i.e., corresponding to perfect antireflection coating. We have checked that the dependence of the results on the actual interchromophore distance is weak within a realistic interchromophore distance range. Apart from the important role light propagation and radiative coupling can play for the nonlinear system dynamics (cf. Sec. III B), explicit consideration of the light propagation also gives direct access to quantities such as transmitted and reflected fractions of light pulses (including amplitude and phase). These quantities retain their relevance in the nonlinear optical regime and are experimentally accessible. Parameters used in the following calculations are summarized in Table I.

We note that in an experiment, stimulated emission in conjugated polymer materials is often studied in a waveguide geometry.[6,64,65] Typically, spin-coated conjugated polymer layers of several hundred nanometer thickness are used to guide the light propagation in the plane of the film. Details of the light-matter interaction strength will depend on the particulars of the waveguide structure used and, since the molecular dipoles are aligned parallel to the plane, the effective interaction strength of the dipoles with the propagating light field will be slightly different compared to the geometry studied here (cf. Fig. 4). This will lead to, e.g., differences in the net gain obtained for a given propagation length. However, we expect the following exploration of nonlinear light pulse propagation through a several-micron-thick spin-coated film, to give representative results illustrating the interplay of nonlinear excitation dynamics and propagation effects.

A. Pump-probe light amplification

To begin with, as an illustrational example, we simplify the considered situation by assuming that the ultrafast excitation dynamics of the β-phase molecules can be studied exclusive from the surrounding α-phase matrix, thus spectral overlap between α and β phases is neglected. We study a system of 500 layers of β-phase chromophores (corresponding to a film thickness of ≈ 8.1 μm with a volume density of β-phase chromophores of 0.43×10^{19} cm^{-3}, cf. Ref. 48). The background refractive index is 1.59, cf. Ref. 49. This system is excited with a series of light pulses. A similar "pump-probe" amplification of pulse trains was studied experimentally in Ref. 5. The pulses are each 1ps long and centered at frequencies 2.942 eV (the first pulse is close to resonance with a transition from the vibronic ground state to the first excited vibrational states of the S_1 electronic state) and 2.638 eV (second and third pulses are close to resonance with a transition from the vibrational ground state of S_1 to the first excited vibrational states of S_0), respectively, as depicted in Fig. 2. Light amplification at these 0-1 vibronic transitions has been observed in isolated polyfluorene chains using a pump-probe experiment[4,66] and in polyfluorene films with a small fraction of beta phase chromophores by detecting amplified spontaneous emission.[37,38,67,68] Figure 5 shows the temporal dynamics of the average total (averaged over the molecular layers and summed over all vibrational states) occupations of the S_0 and S_1 states together with incoming and transmitted pulses for two different relaxation times of vibrational quanta, (a) $t_{\mathrm{rel}}=\hbar/\gamma=1$ ps and (b) $t_{\mathrm{rel}}=20$ ps. The figure shows excitation (pumping) by the first pulse and amplification of the subsequent (probe) pulses as these propagate through the system (the occupation inversion is reduced accordingly). When the second pulse arrives in Fig. 5(a), the excitations induced by the pump pulse have mostly already relaxed to the vibrational ground state of S_1. Since $T=0$, the vibrationally excited states of S_0 are all empty (apart from possible but negligible contributions left from the pumping process). Thus, the second pulse, the "probe" pulse, sees the system in occupation inversion (even real occupation inversion in this case but always occupation inversion between the relevant vibronic states). Accordingly, the probe pulse gets amplified while propagating through the system and the occupation of S_1 gets reduced. For slower vibrational relaxation in Fig. 5(b), when the second pulse

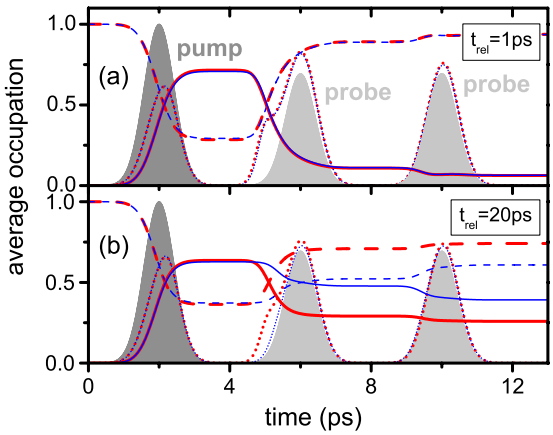

FIG. 5. (Color online) Pump-probe excitation of 8.1μm-thick layer. (a) Average electronic ground (dashed lines), S_0, and excited (solid lines), S_1, state total occupations and incoming (shaded areas), and transmitted (dotted lines) light pulses. (b) As (a) for $t_{\mathrm{rel}}=20$ ps. [(a) and (b)] Results shown for full vibronic (thick/red) and six-level (thin/blue) calculation.

arrives, part of the pumped excited-state occupation still resides in a vibrationally excited state of S_1. In this case the second pulse induces transitions back to the ground state from multiple initial states, resulting in a more complicated dynamics involving multiple vibronic transitions. The third pulse is identical to the second. However, the occupation inversion seen by the third pulse and hence the amplification the third pulse experiences is much weaker than for the second pulse.

Excitation parameters in Fig. 5 are chosen such that optical pumping of the molecular electronic two-level system (coupled to vibrational degrees of freedom) into *real* occupation inversion is achieved which is not a coherent effect here. In an atomic two-level system this behavior is prohibited by Pauli blocking. This highlights a key difference in the molecular excitation dynamics compared to atomic systems. This is enabled by coupling of the electronic states to the vibrational degrees of freedom together with dissipation of vibrational energy. In the molecular material, during the process of optical excitation, part of the vibronic excitations relaxes to vibronic levels lower in energy. Thus, the pump pulse sees an effective vibronic multilevel system, where relaxation redistributes the excitations in energy on a short time scale. This can change the effect of Pauli blocking in the predominantly pumped vibronic states considerably and qualitatively differentiates the optical properties of the molecular system studied from those of a purely electronic system.

To complete this discussion, we compare the results shown in Fig. 5 to a simpler vibronic multilevel calculation where only the three lowest vibrational states are considered for each of the electronic states. Excitation parameters in Fig. 5(a) are chosen such that the simple few-level calculation quite accurately captures the full system dynamics. However, for slower vibrational relaxation as in Fig. 5(b), the simpler model clearly fails to reproduce the more complicated stimulated absorption and emission dynamics of the system and thus also fails to predict the correct shape of the amplified light pulse. This sensitivity to excitation and energy dissipation parameters illustrates that care has to be taken in applying simplified multilevel schemes to these organic systems. Similarly, it has been discussed that gain saturation at high pump intensities and the wavelength shift of the amplified spontaneous emission can only be explained by including vibrational relaxation dynamics in the ground electronic state.[68]

Next, we illustrate the role that light propagation plays in the pulse amplification shown in Fig. 5. For this, we compare with the propagation of the same light pulses through a much thinner (16nm) film. Figure 6 shows the temporally resolved gain in intensity (this is calculated as the difference between transmitted pulse intensity with and without the sample and normalized to the film thickness) for the thin (16nm) and the thick (8.1μm) films. We find significant differences both in the pumping process (first pulse) and in the amplification of the subsequent probe pulses. Overall, the pumping process is slightly less efficient for the thick film, partly because the pulse gets absorbed while penetrating the medium. However, the major difference lies in the dynamics of the excitation: for the thin film, light absorption is strongest for the front

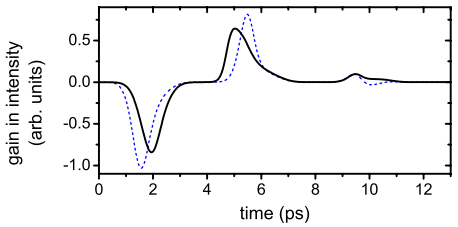

FIG. 6. (Color online) Change in pulse intensity after propagation through a thin (16 nm, dashed line) and a thick (8.1 μm, solid line) film. Same material and excitation parameters as in Fig. 5(a). Shown is the temporally resolved gain in intensity (difference between transmitted pulse intensity with and without the sample) of the pulses for the full vibronic model. For comparison, results are normalized to the sample length. A detailed discussion is given in the text.

part of the pump pulse. At later times, Pauli blocking renders further pumping inefficient. This situation is slightly different in the thicker sample, where, even if at the front of the sample Pauli blocking is efficient, further excitation and thus absorption of the pulse is still possible when the pulse propagates into the sample. For the second pulse, the gain in intensity per propagation length shown in Fig. 6 is very similar for the thin and the thick samples. This is a surprising result as the gain in intensity is commonly expected to grow exponentially with propagation length, not linearly. However, this is only true when the gain medium is not affected by the propagating pulse which is not the case in the strongly nonlinear regime studied here. Also counterintuitive is that the peak of the amplification arrives at earlier times at the end of the thick film than at the end of the thin film. We note that this is not to be interpreted as a superluminal[69] effect (at least not predominantly) but stems from the fact that the pulse front gets much more strongly amplified in the thick sample (due to the light propagation) than in the thin sample. This strong amplification of the pulse front leads to rapid loss of the occupation inversion in the thick sample before most of the pulse hits the sample at later times. In conclusion, the results in Fig. 6 illustrate that the observed amplification is a result of a complicated interplay of nonlinear optical effects and light propagation through the sample. A more detailed analysis of the interplay of nonlinearities between multiple vibronic levels and pulse propagation effects including spectral features will be the subject of future work.

B. Light-propagation effects

In this section, we focus on the role light propagation can play in the excitation dynamics in that it gives rise to ASE.[68] ASE being primarily a stimulated emission effect (only initially spontaneously triggered), we model it by introducing fluctuations in the classical optical field. In the numerical evaluation, enabled by the self-consistent solution of Maxwell and material (density-matrix) equations, the spontaneous radiative decay can be simulated by introducing random fluctuations in the classical light field at each chromophore site. The intensity of this random field contribution is adjusted such that for a single molecule a typical radiative life-

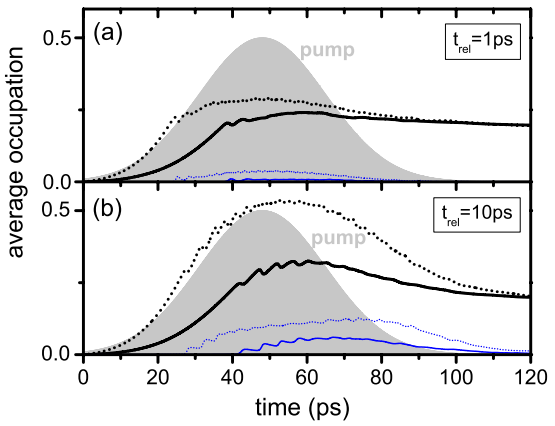

FIG. 7. (Color online) Effects of amplified spontaneous emission on pumping of a $\approx 50\mu$m-thick layer. Shown are the temporal shape of the pump (shaded areas) and average total excited electronic state (thick lines), S_1, and first vibrationally excited electronic ground state (thin lines), S_0, occupations for (a) $t_{\mathrm{rel}}=1$ ps and (b) $t_{\mathrm{rel}}=10$ ps. Dotted lines show results for four times higher pump intensity.

time of the excited state of ≈ 1 ns is obtained (cf. Ref. 36). The fluctuations are included in the spectral range of the 0-1 transitions in emission as this emission is predominantly triggering the ASE in a real system. The spectral amplitude is varied according to the 0-1 emission line shape in Fig. 3(a). We deem this quasiclassical approach sufficient for the purposes of this paper. A more realistic treatment of the quantized light field, without requiring additional constraints on the optical modes, is computationally infeasible.

We study a film of $\approx 50\mu$m thickness ($\hat{=}3000$ layers) that is excited (pumped) with a spectrally narrow 40ps pump pulse (quasi-cw pumping compared to relaxation rates and the time scale on which ASE is observed). In an experiment, the pumping of the β-phase chromophores typically occurs due to efficient and fast (picosecond time scale) excitation transfer from the surrounding glassy phase molecules with larger excitation energies.[68] If the pumping is on a much longer time scale than is needed for the migration to occur, the details of the migration processes are rendered unimportant. Being mostly interested in the dynamics of the stimulated optical emission from the radiatively coupled β-phase chromophores, we imitate the real pumping situation by tuning the center frequency of the pump pulse to 3.4316 meV such that it excites the molecules from the vibronic ground state into a higher excited vibrational state of S_1. Then, the optically induced excitations relax to the bottom of S_1 on a picosecond time scale. Figure 7 shows the time dynamics of the average total excited-state population. With increasing occupation of S_1, ASE from the lowest vibrational level of S_1 to the first excited vibrational levels of S_0 becomes important, manifested in the finite occupation of the vibrationally excited states of S_0. The role of ASE increases with increasing film thickness and thus propagation length (not shown).[41] Also shown is the result with four times higher pump intensity. Only a slight increase in excited-state occupation is found for $t_{\mathrm{rel}}=1$ ps in Fig. 7(a) (ASE is more efficient for faster relaxation of vibrational quanta). We would further like to note that the maximum occupation inversion reached in Fig. 7 is higher for slower vibrational relaxation thus when ASE is less efficient. Without ASE included in the calculations, the opposite result is found (not shown). However, with ASE, rapid vibrational relaxation depopulates the predominantly pumped state and thus reduces Pauli blocking that hinders the pumping process. These results illustrate the role of ASE as a limiting factor in reaching high occupation inversion in high-gain extended molecular systems. For sufficiently strong ASE, rapid (spontaneous) recombination of part of the excitations occurs resulting in a complicated dynamical interplay of relaxation oscillations [more pronounced in Fig. 7(b)] and Pauli blocking between various vibronic states.

IV. REMARKS AND CONCLUSIONS

We have introduced a powerful theoretical approach for microscopic modeling of the nonlinear optical excitation dynamics of organic semiconductor (conjugated polymer) systems. Our approach combines the flexibility of a density-matrix-theory approach (in part motivated by the great success of density-matrix-theory approaches in the optics of inorganic semiconductor systems) applicable to realistic systems, with the power of ab initio quantum-chemistry calculations for a given molecular system. This unique combination of both density-matrix theory and ab initio quantum-chemistry potentially leads to predictive capabilities for nonlinear optical properties of a wide range of relevant conjugated polymer systems. Beyond modeling the nonlinear optical response of a molecular system, we have shown that light propagation can be readily included. The theory allows one to follow the spatiotemporal dynamics of the optically induced occupations (diagonal elements of the density matrix) and polarizations (off-diagonal elements of the density matrix) on ultrashort time scales.

We have explicitly demonstrated the application of our general approach to a conjugated polymer guest-host material of great current interest: polyfluorene containing a small amount of β-phase chromophores. For this system we have discussed the ultrafast photoexcitation dynamics and illustrated the importance of light propagation in that it, for example, gives rise to amplified spontaneous emission. We predict reshaping of amplified optical pulses propagating through polyfluorene films containing a small content of β-phase molecules and expose the limitations of a simple multilevel scheme. Oscillatory structures in the amplified spontaneous emission in a thick ($\approx 50\mu$m) film are also observed, features whose origin lies in the rich underlying electronic and vibrational population and polarization dynamics.

As straightforward extensions of the present work, detailed studies of the pulse reshaping reported, a comprehensive analysis of the spatiotemporal excitation dynamics, and the discussion of spectral features such as frequency-dependent phase shifts are subjects for future work. Beyond these results, we envision that in future studies our approach will be extended and applied to study a variety of physical effects in organic materials and that it has the potential to be adapted to study realistic polymer optoelectronic and photonic devices.

ACKNOWLEDGMENTS

We gratefully acknowledge continuous helpful discussions with Martin Paterson, Heriot-Watt University. This work was supported by the Engineering and Physical Sciences Research Council (EPSRC).

APPENDIX: RELAXATION AND DEPHASING

In this appendix we give the explicit expressions for relaxation and dephasing terms that are included in the solution of Eq. (8). Each oscillator mode is coupled to a bath with temperature T and corresponding mean vibrational occupation number $\bar{n}$. The relaxation terms follow from Eq. (9) and are given in matrix representation in the basis of the oscillator modes of the electronic ground state S_0. β_i is the displacement of the considered normal mode of the i^{th} PES relative to the PES of S_0. We use the following abbreviation: $\tilde{\rho}_{ij}=\text{Re}\{\rho_{ij}\}$. The relaxation then takes the following form:

$$\begin{aligned}\dot{\rho}^{ii}_{\nu,\nu'}|_{\text{relax.}} = \gamma[&(\nu+\nu')\tilde{\rho}^{ii}_{\nu,\nu'} - 2\sqrt{\nu+1}\sqrt{\nu'+1}\tilde{\rho}^{ii}_{\nu+1,\nu'+1} \\ &+ \beta_i(\sqrt{\nu}\tilde{\rho}^{ii}_{\nu-1,\nu'} + \sqrt{\nu'}\tilde{\rho}^{ii}_{\nu,\nu'-1} - \sqrt{\nu+1}\tilde{\rho}^{ii}_{\nu+1,\nu'} \\ &- \sqrt{\nu'+1}\tilde{\rho}^{ii}_{\nu,\nu'+1}) + 2\bar{n}\{(\nu+\nu'+1)\tilde{\rho}^{ii}_{\nu,\nu'} \\ &- \sqrt{\nu+1}\sqrt{\nu'+1}\tilde{\rho}^{ii}_{\nu+1,\nu'+1} - \sqrt{\nu}\sqrt{\nu'}\tilde{\rho}^{ii}_{\nu-1,\nu'-1}\}].\end{aligned}$$

The dephasing of polarizations between electronic states $i \neq j$ is

$$\begin{aligned}\dot{\rho}^{ij}_{\nu,\nu'}|_{\text{deph.}} = 2\gamma\{&[(\nu+\nu'+\beta_i^2+\beta_j^2)\tilde{\rho}^{ij}_{\nu,\nu'} + \beta_i(\sqrt{\nu}\tilde{\rho}^{ij}_{\nu-1,\nu'} \\ &+ \sqrt{\nu+1}\tilde{\rho}^{ij}_{\nu+1,\nu'}) + \beta_j(\sqrt{\nu'}\tilde{\rho}^{ij}_{\nu,\nu'-1} + \sqrt{\nu'+1}\tilde{\rho}^{ij}_{\nu,\nu'+1})] \\ &\times(2\bar{n}+1) + 2\bar{n}\tilde{\rho}^{ij}_{\nu\nu'}\} + \gamma_{\text{pure}}\rho^{ij}_{\nu,\nu'}.\end{aligned}$$

This dephasing includes the dephasing introduced by vibrational relaxation and an additional relaxation-independent pure dephasing γ_{pure}.

*Corresponding author; i.galbraith@hw.ac.uk

[1] *Polyfluorenes*, Advances in Polymer Science Vol. 212, edited by U. Scherf and D. Neher (Springer, Berlin, 2008).
[2] E. Collini and G. Scholes, Science **323**, 369 (2009).
[3] Y.-S. Huang, S. Westenhoff, I. Avilov, P. Sreearunothai, J. M. Hodgkiss, C. Deleener, R. H. Friend, and D. Beljonne, Nature Mater. **7**, 483 (2008).
[4] T. Virgili, D. Marinotto, G. Lanzani, and D. D. C. Bradley, Appl. Phys. Lett. **86**, 091113 (2005).
[5] D. Amarasinghe, A. Ruseckas, A. E. Vasdekis, G. A. Turnbull, and I. D. W. Samuel, Adv. Mater. **21**, 107 (2009).
[6] D. Amarasinghe, A. Ruseckas, G. A. Turnbull, and I. D. W. Samuel, Proc. IEEE **97**, 1637 (2009).
[7] I. D. W. Samuel and G. A. Turnbull, Chem. Rev. **107**, 1272 (2007).
[8] S. Perissinotto, G. Lanzani, M. Zavelani-Rossi, M. Salemo, and G. Gigli, Appl. Phys. Lett. **91**, 191108 (2007).
[9] G. Tsiminis, A. Ruseckas, I. D. W. Samuel, and G. A. Turnbull, Appl. Phys. Lett. **94**, 253304 (2009).
[10] F. Jahnke *et al.*, Phys. Rev. Lett. **77**, 5257 (1996).
[11] J. Z. Zhang and I. Galbraith, Appl. Phys. Lett. **84**, 1934 (2004).
[12] J. V. Moloney, J. Hader, and S. W. Koch, Laser Photonics Rev. **1**, 24 (2007).
[13] S. Schumacher, N. H. Kwong, R. Binder, and A. L. Smirl, Phys. Status Solidi (RRL) **3**, 10 (2009).
[14] H. Haug and S. W. Koch, *Quantum Theory of the Optical and Electronic Properties of Semiconductors*, 3rd ed. (World Scientific, Singapore, 1995).
[15] G. Khitrova, H. M. Gibbs, F. Jahnke, M. Kira, and S. W. Koch, Rev. Mod. Phys. **71**, 1591 (1999).
[16] M. Lorke, F. Jahnke, and W. W. Chow, Appl. Phys. Lett. **90**, 051112 (2007).
[17] W. P. Su, J. R. Schrieffer, and A. J. Heeger, Phys. Rev. Lett. **42**, 1698 (1979).
[18] S. Mukamel, S. Tretiak, T. Wagersreiter, and V. Chernyak, Science **277**, 781 (1997).
[19] M. Rohlfing and S. G. Louie, Phys. Rev. Lett. **82**, 1959 (1999).
[20] S. Karabunarliev, E. R. Bittner, and M. Baumgarten, J. Chem. Phys. **114**, 5863 (2001).
[21] J. Gierschner, H.-G. Mack, L. Lüer, and D. Oelkrug, J. Chem. Phys. **116**, 8596 (2002).
[22] G. D. Scholes and G. Rumbles, Nature Mater. **5**, 683 (2006).
[23] T. Meier, S. Tretiak, V. Chernyak, and S. Mukamel, Phys. Rev. B **55**, 4960 (1997).
[24] V. M. Axt and S. Mukamel, Rev. Mod. Phys. **70**, 145 (1998).
[25] V. May and O. Kühn, *Charge and Energy Transfer Dynamics in Molecular Systems*, 2nd ed. (Wiley-VCH, Weinheim, 2003).
[26] D. Egorova, M. F. Gelin, M. Thoss, H. Wang, and W. Domcke, J. Chem. Phys. **129**, 214303 (2008).
[27] H. Zhao, S. Mazumdar, C. X. Sheng, M. Tong, and Z. V. Vardeny, Phys. Rev. B **73**, 075403 (2006).
[28] D. O'Carroll, D. Iacopino, A. O'Riordan, P. Lovera, E. O'Connor, G. A. O'Brien, and G. Redmond, Adv. Mater. **20**, 42 (2008).
[29] J. Peet, E. Brocker, Y. Xu, and G. C. Bazan, Adv. Mater. **20**, 1882 (2008).
[30] W. C. Tsoi, A. Charas, A. J. Cadby, G. Khalil, A. M. Adawi, A. Iraqi, B. Hunt, J. Morgado, and D. G. Lindzey, Adv. Funct. Mater. **18**, 600 (2008).
[31] J. Morgado and L. Alcacer, Appl. Phys. Lett. **90**, 201110 (2007).
[32] E. Da Como, K. Becker, J. Feldmann, and J. M. Lupton, Nano Lett. **7**, 2993 (2007).
[33] E. Da Como, E. Scheler, P. Strohriegl, J. M. Lupton, and J. Feldmann, Appl. Phys. A: Mater. Sci. Process. **95**, 61 (2009).
[34] I. Franco and S. Tretiak, J. Am. Chem. Soc. **126**, 12130 (2004).
[35] C. Rothe, F. Galbrecht, U. Scherf, and A. Monkman, Adv. Mater. **18**, 2137 (2006).
[36] S. Schumacher, A. Ruseckas, N. A. Montgomery, P. J. Skabara, A. L. Kanibolotsky, M. J. Paterson, I. Galbraith, G. A. Turnbull, and I. D. W. Samuel, J. Chem. Phys. **131**, 154906 (2009).
[37] M. Anni, Appl. Phys. Lett. **93**, 023308 (2008).
[38] M. Anni and M. Alemanno, Phys. Rev. B **78**, 233102 (2008).

[39] M. Richter, T. Renger, and A. Knorr, Photosynth. Res. **95**, 119 (2008).
[40] M. Richter, G. Th. Renger, and A. Knorr, J. Chem. Phys. **127**, 075105 (2007).
[41] A. E. Siegman, *Lasers* (University Science Books, Sausalito, CA, 1986).
[42] G. Juzeliūnas and J. Knoester, J. Chem. Phys. **112**, 2325 (2000).
[43] M. Richter, K. J. Ahn, A. Knorr, A. Schliwa, D. Bimberg, M. E.-A. Madjet, and T. Renger, Phys. Status Solidi B **243**, 2302 (2006).
[44] G. Lindblad, Commun. Math. Phys. **48**, 119 (1976).
[45] D. Gelman, G. Katz, R. Kosloff, and M. A. Ratner, J. Chem. Phys. **123**, 134112 (2005).
[46] T. Tawara, H. Kamada, T. Tanabe, T. Sogawa, H. Okamoto, P. Yao, P. K. Pathak, and S. Hughes, Opt. Express **18**, 2719 (2010).
[47] M. F. Gelin, D. Egorova, and W. Domcke, J. Chem. Phys. **131**, 124505 (2009).
[48] A. L. T. Khan, P. Sreearunothai, L. M. Herz, M. J. Banach, and A. Köhler, Phys. Rev. B **69**, 085201 (2004).
[49] M. Campoy-Quiles, G. Heliotis, R. Xia, M. Ariu, M. Pintani, P. Etchegoin, and D. D. C. Bradley, Adv. Funct. Mater. **15**, 925 (2005).
[50] G. Ryu, P. N. Stavrinou, and D. D. C. Bradley, Adv. Funct. Mater. **19**, 3237 (2009).
[51] J. B. Foresman and A. Frisch, *Exploring Shemistry With Electronic Structure Methods* (Gaussian, Pittsburgh, 1996).
[52] E. Jansson, P. C. Jha, and H. Agren, Chem. Phys. **336**, 91 (2007).
[53] J. P. Schmidtke, J.-S. Kim, J. Gierschner, C. Silva, and R. H. Friend, Phys. Rev. Lett. **99**, 167401 (2007).
[54] J. M. Winfield, A. Van Vooren, M. J. Park, D. H. Hwang, J. Cornil, J. S. Kim, and R. H. Friend, J. Chem. Phys. **131**, 035104 (2009).
[55] X. Ma and W. Rhodes, Phys. Rev. A **41**, 4625 (1990).
[56] X. Ma and W. Rhodes, Phys. Rev. A **39**, 1941 (1989).
[57] S. Banerjee and G. Gangopadhyay, Chem. Phys. Lett. **359**, 295 (2002).
[58] W. Chunwaschirasiri, B. Tanto, D. L. Huber, and M. J. Winokur, Phys. Rev. Lett. **94**, 107402 (2005).
[59] R. Scholz, L. Gisslen, C. Himcinschi, I. Vragovic, E. M. Calzado, E. Louis, E. S. F. Maroto, and M. A. Diaz-Garcia, J. Phys. Chem. A **113**, 315 (2009).
[60] G. Heimel, M. Daghofer, J. Gierschner, E. J. W. List, A. C. Grimsdale, K. Müllen, D. Beljonne, J. Bredas, and E. Zojer, J. Chem. Phys. **122**, 054501 (2005).
[61] Z. S. Yang, N. H. Kwong, R. Binder, and A. L. Smirl, J. Opt. Soc. Am. B **22**, 2144 (2005).
[62] S. Schumacher, N. H. Kwong, and R. Binder, Appl. Phys. Lett. **92**, 131109 (2008).
[63] M. Wegener, J. L. Garcia-Pomar, C. M. Soukoulis, N. Meinzer, M. Ruther, and S. Linden, Opt. Express **16**, 19785 (2008).
[64] E. M. Calzado, J. M. Villalvilla, P. G. Boj, J. A. Quintana, and M. A. Díaz García, J. Appl. Phys. **97**, 093103 (2005).
[65] T. Virgili, J. Clark, J. Cabanillas-Gonzalez, L. Bazzana, K. C. Vishnubhatla, R. Osellame, R. Ramponi, and G. Lanzani, J. Mater. Chem. **20**, 519 (2010).
[66] T. Virgili, D. Marinotto, C. Manzoni, G. Cerullo, and G. Lanzani, Phys. Rev. Lett. **94**, 117402 (2005).
[67] G. Ryu, R. Xia, and D. D. C. Bradley, J. Phys.: Condens. Matter **19**, 056205 (2007).
[68] M. Anni and M. Alemanno, Appl. Phys. Lett. **93**, 123311 (2008).
[69] R. W. Boyd and D. J. Gauthier, Science **326**, 1074 (2009).